Available online at www.sciencedirect.com
ScienceDirect
Catalysis Today 136 (2008) 190–205
CATALYSIS TODAY
www.elsevier.com/locate/cattod

Diesel fuel reforming using catalytic membrane reactors☆

M.V. Mundschau *, Christopher G. Burk, David A. Gribble Jr.

Eltron Research & Development Inc., 4600 Nautilus Court South, Boulder, CO 80301-3241, United States[1]

Available online 28 March 2008

Abstract

Reactors incorporating porous membranes of yttria-stabilized zirconia combined with beds of perovskite oxidation catalysts are being developed to convert pump-grade, low-sulfur diesel fuel into synthesis gas. Purified mixtures of H_2 and CO might be used to power solid-oxide fuel cells (SOFCs), or the hydrogen could be used as a reductant in diesel automotive pollution control devices. Air is transported into reactors through porous cylindrical reactor walls. A very high local partial pressure of oxygen is maintained near the inner reactor walls to thermodynamically disfavor formation of carbon on reactor surfaces, especially along the cool zones of the fuel feed. The reactor hot zone, which contains a bed of perovskite catalyst, is operated at or above 950 °C and under conditions which thermodynamically suppress formation of carbon. Perovskite catalysts, $La_{0.5}Sr_{0.5}CoO_{3-\delta}$ and $La_{0.5}Sr_{0.5}FeO_{3-\delta}$, show tolerance to sulfur and high activity for reforming diesel fuel, the latter being more stable under reducing conditions. Under the appropriate thermodynamic conditions, cobalt and iron catalyze Fischer-Tropsch reactions in reverse, transforming hydrocarbons into hydrogen and carbon monoxide. The perovskite catalysts are designed to incorporate lattice vacancies, allowing high oxygen-anion mobility and oxidation of adsorbed carbonaceous materials from beneath. The perovskites are mixed electron-anion conductors also designed for high mobility of electrons required for electron transfer reactions. Platinum–rhodium wire gauze operated above 950 °C shows good tolerance to sulfur and high activity for oxidation of diesel fuel and is used as a baseline for comparison of activity of the perovskite catalysts. In excess oxygen, the perovskites catalyze the complete oxidation of diesel fuel into CO_2 and water and are comparable in activity to that of the noble metals. Perovskite oxidation catalysts may find application in pollution control.

Keywords: Diesel fuel reforming; Membrane reactor; Perovskites; Pollution control

1. Introduction

This paper discusses reforming of diesel fuel into synthesis gas, a mixture of $H_2 + CO$. The synthesis gas, after sufficient removal of sulfur and other impurities, might be utilized in solid-oxide fuel cells (SOFCs), and the hydrogen might be used in pollution control devices designed for diesel engines. Fuel reformers combined with water-gas shift reactors to increase hydrogen production by the reaction: $CO + H_2O = CO_2 + H_2$ and equipped with dense hydrogen transport membranes [1–4], could provide hydrogen of sufficient purity for proton-exchange-membrane (PEM) fuel cells.

A major issue in reforming of diesel fuel is the deposition of carbon onto reactor walls and catalysts. To eliminate deposition of carbon onto reactor walls, a membrane reactor is being developed in which air is introduced into the reformer through porous reactor walls [5]. Oxygen is maintained at very high partial pressures near the inner reactor walls and suppresses the deposition of carbon in the cool zones of the reactor feed. Walls of the membrane reactors are designed to be self-cleaning.

Catalysts in the reactor hot zone contain cobalt and iron incorporated into oxides with the perovskite crystal structure (see Fig. 1) [6–9]. Cobalt and iron, long used in Fischer-Tropsch synthesis of hydrocarbons from H_2 and CO [10,11], also catalyze the reverse reactions and transform hydrocarbons into synthesis gas. To suppress deposition of carbon, the perovskite catalysts are doped to produce oxygen lattice vacancies. Vacancies enhance diffusion of oxygen anions through the bulk oxide materials and allow deposited carbon to be attacked by oxygen from beneath.

☆ Presented at 234th ACS National Meeting, Division of Fuel Chemistry, Boston, Massachusetts. Session: Fuel Processing for Hydrogen Production: Reforming of Hydrocarbon Fuels, Paper No. 119740, 19 August 2007.

* Corresponding author. Tel.: +1 303 530 0263; fax: +1 303 530 0264.
E-mail address: mmundschau@eltronresearch.com (M.V. Mundschau).
[1] eltron@eltronresearch.com.

0920-5861/$ – see front matter © 2008 Elsevier B.V. All rights reserved.
doi:10.1016/j.cattod.2008.02.003

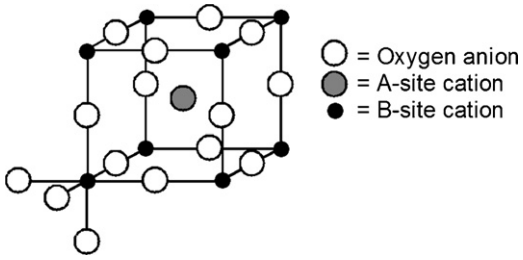

Fig. 1. Ideal cubic perovskite crystal lattice. A-sites are occupied by larger-diameter cations including La^{3+}, Sr^{2+}, and Ca^{2+}. B-sites are occupied by smaller transition elements such as Fe^{3+}, Fe^{2+}, Co^{3+}, Co^{2+} Mn^{3+}, Ru^{3+}, etc.

1.1. Thermodynamic considerations

Fig. 2 shows results of thermodynamic calculations for a diesel fuel mixture containing an empirically analyzed atomic ratio of H:C of 1.86:1 and using a stoichiometric ratio of one atom of oxygen for each atom of carbon to form CO in the reaction: $H_{1.86}C + 0.5\ O_2 = 0.93\ H_2 + CO$. Calculations predict that the desired products, $H_2 + CO$, will be overwhelmingly favored *if the system can be brought to equilibrium* at or above about 950 °C. Deep oxidation products, H_2O and CO_2, if formed initially, will not be stable at higher temperatures if the system can be brought to equilibrium. It should be noted that diesel fuel, because of its lower hydrogen-to-carbon atomic ratio, requires higher reforming temperatures relative to methane (CH_4), which has a higher H:C atomic ratio of 4:1. Likewise, other alkanes with higher hydrogen-to-carbon atomic ratios can be reformed at slightly lower temperatures without thermodynamically favoring deposition of carbon. Conversely, coal with lower hydrogen content will require higher gasification temperatures.

Calculations also predict that elemental carbon will be the favored product at lower temperatures (see left side of Fig. 2). A major challenge in the reforming of diesel fuel is the avoidance of the deposition of carbon onto walls in the cool zones of the reactor, especially as the fuel is heated to the desired reforming temperature above 950 °C. Furthermore, if the synthesis gas, once formed, is cooled below the desired reforming temperature, deposition of carbon will be favored in the exhaust lines by the Boudouard reaction: $2CO = C + CO_2$, if the walls of the exhaust lines are not catalytically inert. Likewise, undesired products, CH_4, CO_2 and H_2O, will be thermodynamically favored in cooler exhaust lines if the walls are not catalytically inert. Although the calculations predict that the mole fraction of carbon will be relatively minor between 800 and 900 °C, this will be far from negligible as far as reforming catalysts are concerned, which can be deactivated if coated by even a few monolayers of carbon.

Diesel fuel is a mixture which may contain approximately 400 distinct hydrocarbons, some 20 organic compounds of sulfur, and additives. The distribution of the carbon number of the hydrocarbon molecules peaks in the range of 15–25 carbon atoms per molecule (C_{15}–C_{25}) [12]. Aromatic compounds may comprise 20 vol.% of the mixture. Cracking of alkanes during reforming may form additional aromatic molecules. Diesel fuel and its decomposition products can include polycyclic aromatic molecules such as naphthalene ($C_{10}H_8$), anthracene ($C_{14}H_{10}$), pyrene ($C_{16}H_{10}$), and benzo[*a*]pyrene ($C_{20}H_{12}$), containing two, three, four and five fused benzene rings, respectively [13]. The polycyclic aromatic compounds may also have attached side chains of methyl, ethyl or other alkyl radicals. The H:C atomic ratio of the aromatic compounds is lower relative to that of alkanes (for example, 0.8:1 in naphthalene; 0.6:1 in benzo[*a*]pyrene), implying the need for a higher reforming temperature if a residuum of aromatic compounds collects in the reactor after the easy-to-reform alkanes have been reacted and some hydrogen removed. Nuclei for growth of graphitic residues may evolve from polycyclic aromatic compounds upon loss of hydrogen [13]. Once nucleated, carbonaceous deposits are autocatalytic; they catalyze their own formation. Exponential growth of carbon under both thermodynamically and kinetically favored conditions leads to rapid plugging of reactors and catalyst beds. Nuclei may form not only on reactor walls and catalyst surfaces but may also form in the gas phase, and the soot swept to the catalyst beds.

The least stable components of diesel fuel crack into free radicals at the auto-ignition temperature, which may be as low as 250 °C for some fuels. If insufficient oxygen is present, the free radicals can initiate chain polymerization reactions forming tars. The least stable compounds will crack before they can volatilize. The inability to easily volatilize all

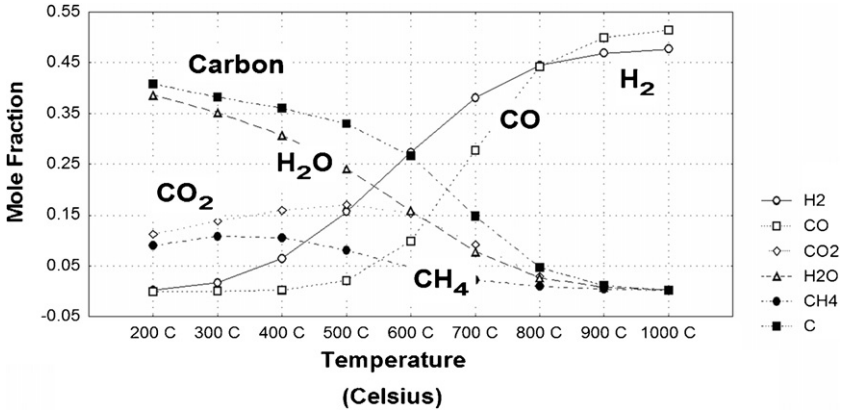

Fig. 2. Results of thermodynamic calculations for reforming diesel fuel into syngas. The desired products, H_2 and CO, will be overwhelmingly favored if the system can be brought to equilibrium above about 950 °C. Carbon will form as fuel is heated, if precautions are not taken.

components of diesel fuel before they crack adds to the difficulty of reformation. The relatively non-volatile nature of diesel fuels, commercial jet fuels, and military JP-8 fuels (Jet Propulsion #8), is preferred in aviation and military applications because of reduced fire and explosion hazard. Unlike volatile gasoline, which in gasoline engines is readily converted into the gaseous state and ignited in the vapor state, diesel fuel is injected into diesel engines in the liquid state after air is heated to fuel combustion temperatures by the adiabatic compression stroke of the pistons. In fact, Rudolf Diesel had envisioned injection and ignition of un-refined crude petroleum and even pulverized coal in his early engines [14].

In general, increasing the H:C or the O:C atomic ratio in the reformate will lower the reforming temperature needed to thermodynamically suppress formation of carbon [15]. Recirculation of steam and CO_2 from fuel cell exhaust also will suppress carbon deposition in fuel reformers by the reactions: $H_2O + C = H_2 + CO$ and $CO_2 + C = 2CO$ (reverse Boudouard reaction) [15]. Recirculation of unconsumed H_2 from fuel cell exhaust likewise will suppress deposition of carbon. Increasing the O:C atomic ratio beyond the desired stoichiometric ratio of 1:1 by increasing the flow of molecular oxygen from air will also lower the reforming temperature required to suppress formation of carbon. However, a significant fraction of the H_2 and CO will be oxidized to $H_2O + CO_2$ as carbon is oxidized to CO or CO_2, and this will reduce reformer efficiency. Reforming temperature can also be lowered if oxygen is added to the diesel fuel in the form of oxygenates. Fischer-Tropsch products containing long-chain aliphatic alcohols [11] or biodiesel containing methyl esters of fatty acids will aid suppression of carbon if blended with petroleum-based diesel fuels.

In the present research, the method devised to suppress the deposition of carbon on reactor walls of the feed is to introduce air into the system through porous walls of yttria-stabilized zirconia (YSZ), thus maintaining a very high local concentration of oxygen near the inner walls of the cool zones of the reactor feed. Fig. 3 summarizes schematically the calculated oxygen-to-carbon atomic ratios required along the inner walls to completely suppress deposition of carbon at various temperatures at equilibrium. The research goal is to maintain very high *local*

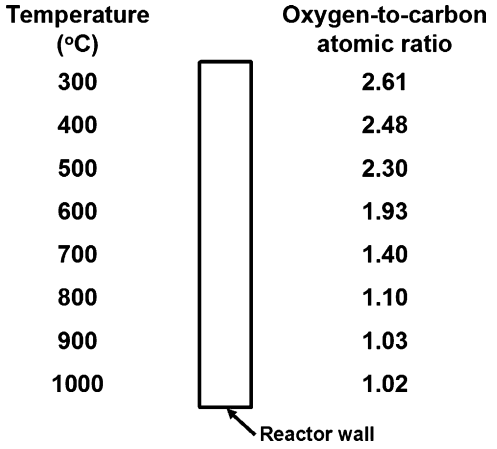

Fig. 3. Calculated local atomic ratio of O:C needed at inner reactor walls to completely suppress deposition of carbon.

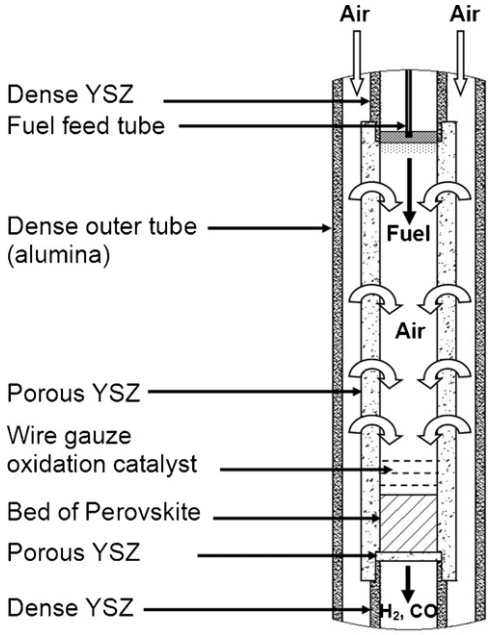

Fig. 4. Schematic of porous, self-cleaning wall in which air is brought into the system through porous membranes of yttria-stabilized zirconia (YSZ).

concentrations of oxygen near the inner walls but to maintain an overall O:C atomic ratio of near 1:1 in the system as the fuel/air mixture reaches the reactor hot zone. The 1:1 atomic ratio maximizes production of synthesis gas without sacrificing a large fraction of the fuel to deep oxidation. Fig. 4 shows schematically the concept of the porous membrane reactor.

1.2. Selection of sulfur-tolerant reforming catalysts

Sulfur in diesel fuel is a potential poison for many reforming catalysts, as well as for catalysts in fuel cells. The concentration of sulfur in so-called ultra-low sulfur diesel fuel is limited by law in the United States (as of January 2007) to a maximum of 15 ppm by mass. However, this is still too high to avoid poisoning of many catalysts. In the search for sulfur-tolerant catalysts, it is useful to refer to Ellingham Diagrams (see Fig. 5), which plot Gibbs' free energy of formation of various bulk sulfides as a function of temperature and H_2S/H_2 molar ratio in the system [16,17]. Also drawn in Fig. 5 (broader lines) are lines for H_2S/H_2 molar ratios expected in reformates derived from JP-8 (Jet Propulsion #8) containing 5000 ppmw sulfur and commercial diesel fuel containing 15 ppmw sulfur. Bulk metal sulfides above the lines drawn for specific H_2S/H_2 molar ratios in the reformate will be unstable relative to H_2S and will react by the general equation: $MS + H_2 = M + H_2S$, where M represents a reduced metal and MS a generalized metal sulfide. Metallic elements below the lines of a given H_2S/H_2 molar ratio will be unstable with respect to metal sulfides and will react with H_2S by the generalized equation: $M + H_2S = MS + H_2$.

From Fig. 5, it is predicted that platinum and iridium should not form stable bulk sulfides if held at temperatures above about 800 °C—even with levels of sulfur contained in JP-8. In the case of diesel fuel containing 15 ppmw sulfur, elements including Ir, Pt, Ag, W, Mo, Co and Fe should not form stable

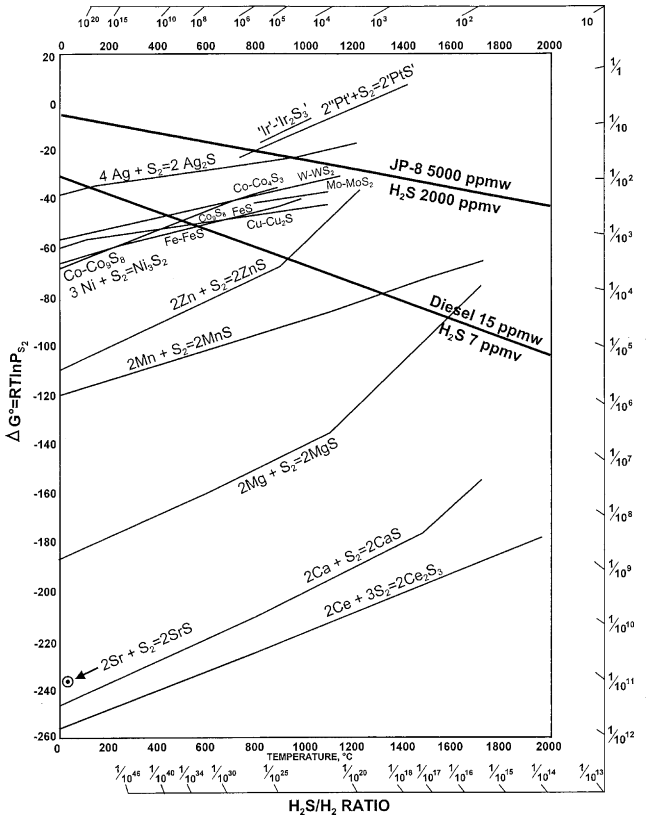

Fig. 5. Ellingham diagram plotting the standard Gibbs' free energy of formation of selected sulfides.

bulk sulfides at desired reforming temperatures near 950 °C and are candidates for sulfur tolerant catalysts. However, these elements might still be poisoned by monolayers of sulfur, but such poisoning may be reversible and will be less severe relative to formation of bulk sulfides. In general, to desorb sulfur adsorbed in monolayers, temperatures will be required above that of bulk sulfide decomposition.

From this analysis, iron and cobalt were selected as potential base-metal sulfur-tolerant catalysts. Tungsten and molybdenum were not selected because of possible issues with volatile oxides. Silver and copper were not selected because of concerns with melting points and vapor pressures. Of the noble metals, platinum was predicted to be a good potential sulfur-tolerant catalyst at elevated temperatures. (*Note*: It should be appreciated that sulfur is a potent poison for Pt at lower temperature or with low hydrogen partial pressures.) Platinum–rhodium wire gauze, which has long been used in chemical industry to oxidize ammonia to NO_2, for example, [18] was deemed superior to unalloyed Pt. (Although Rh is not shown in standard Ellingham diagrams, bulk sulfides of rhodium are unstable relative to most base metals.)

Platinum–rhodium wire gauze has the advantage that it can be cycled between reducing conditions and exposure to air without danger of forming a bulk oxide. The extreme melting points of Pt (1772 °C) and Rh (1966 °C) allow use of the wire gauze well above 1000 °C in the thermodynamically desired temperature region favorable for syngas production (see Fig. 2). Unlike finely dispersed Pt/Rh bimetallic catalysts supported on zirconia, which were found in the authors' earlier research to deactivate at 1000 °C by sintering, Pt–Rh gauze has low initial surface area and is stable. Disadvantages of the Pt–Rh gauze include high cost. Sufficient gauze must be employed to bring the system to equilibrium in order to avoid kinetic control which favors deep oxidation of hydrogen to water and CO to CO_2.

Due to the pyrophoric nature of highly dispersed base metals of cobalt or iron on conventional oxide supports such as alumina or zirconia, cobalt and iron were incorporated into oxides with the perovskite crystal structure. The perovskites are refractory oxides and are extremely stable under strongly oxidizing conditions. Use of perovskites allows the catalysts to be cycled between reducing conditions and exposure to air.

Referring again to Fig. 5, elements showing very negative Gibbs' free energy of formation of sulfides (Zn, Mn, Mg, Ca and Ce) are predicted to strongly bind sulfur and to form very stable bulk sulfides. They are excellent candidates for use as getters in catalyst guard beds used to strongly bind and remove sulfur, or they may be used in catalyst supports to draw sulfur away from the catalytically active metals.

2. Experimental

2.1. Apparatus

Fig. 6 is a photograph of a porous YSZ tube used to effuse air into the reactor. Yttria-stabilized zirconia was chosen as the porous wall material because of its refractory nature (melting point of pure ZrO_2 is 2715 °C) and the lower likelihood of poisoning nickel catalysts of SOFCs by volatile components issuing from less refractory materials such as porous stainless steel. Yttria-stabilized zirconia is used as the solid-state electrolyte in SOFCs and is in physical contact with the nickel catalysts at elevated temperatures. Like the solid-state YSZ electrolyte, the porous yttria-stabilized zirconia, which is used in the walls of the fuel reformer, contains oxygen-anion vacancies, which enhance diffusion of oxygen by a vacancy-hopping mechanism [19]. Zirconia was also chosen to avoid acid surface sites, such as those of alumina and silica [20], which are known to catalyze cracking of hydrocarbons. In addition, silica, which is often used as a sintering aid in many types of alumina, can be hydrothermally transported by steam in reactors and can poison fuel cell catalysts and reforming catalysts placed in the hot zone of the reformer.

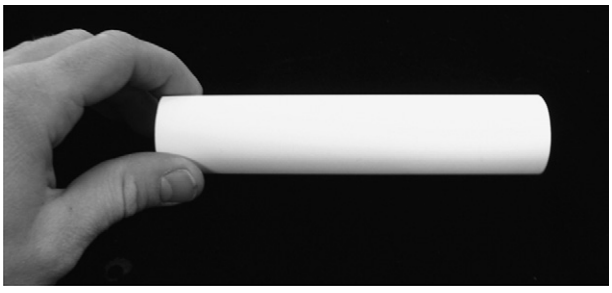

Fig. 6. A tube of porous yttria-stabilized zirconia used in the membrane reactor.

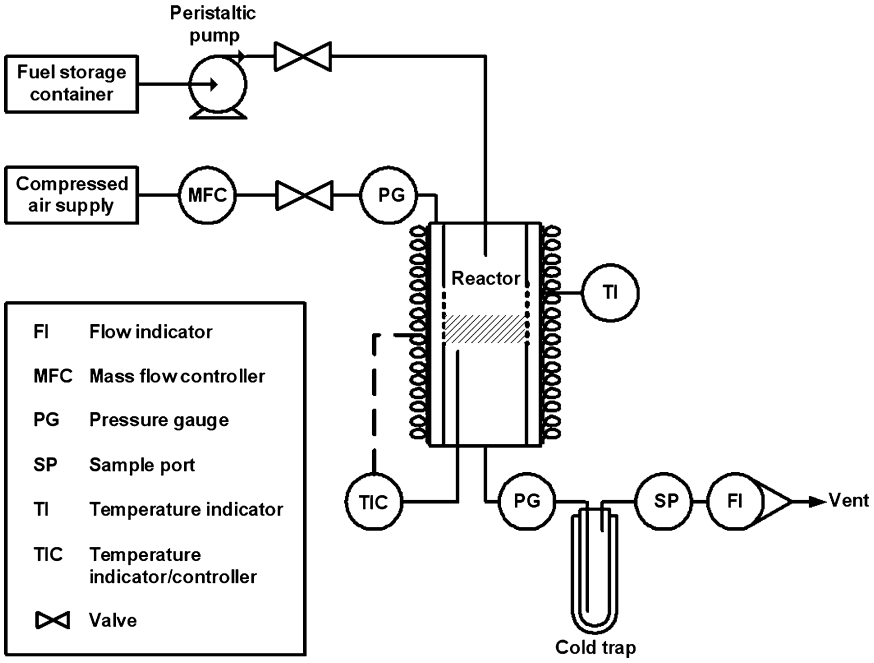

Fig. 7. Schematic of laboratory apparatus for reforming diesel fuel.

Fig. 7 is a schematic of the laboratory apparatus used to test the porous membranes and the diesel fuel reforming catalysts. A 550 W tube furnace capable of reaching 1100 °C surrounds the reactor. The furnace temperature is controlled by a signal from a thermocouple located in the reformate exhaust and positioned approximately 1 cm below the catalyst bed of the hot zone. A second thermocouple located in the middle of the tube furnace monitors the maximum furnace temperature outside of the reactor. A Masterflex L/S® peristaltic cartridge pump (Model 8519–10) feeds diesel fuel into the reactor through a 316 stainless steel tube (o.d. 1.59 mm, i.d. 0.64 mm). The opening of the diesel fuel feed tube is positioned approximately 13 cm above the catalyst bed in the hot zone. The peristaltic pump is calibrated by weighing liquid samples dispensed in a unit time.

Referring to Fig. 4, the inner cylinder has three interlocking sections with the porous yttria-stabilized zirconia membrane in the center and dense tubes in the upper feed and lower exhaust sections. The outer tube surrounding the porous YSZ membrane is of dense alumina. Dense YSZ is preferred for all three dense tubes, but for cost advantages, dense alumina tubes are used in the present experimental apparatus. Modified stainless steel Swagelok fittings, with in-house machined Teflon ferrules kept outside the furnace and used below 280 °C, seal and secure the tube assemblies. A porous YSZ disc, 22.2 mm (0.875 in.) in diameter and 3.2 mm (0.125 in.) in thickness, supports the perovskite catalyst bed of the hot zone.

Custom-machined YSZ porous tubes (see Fig. 6), 15.24 cm (6 in.) in length, 1.90 cm (0.75 in.) in inner diameter and 3.18 cm (1.25 in.) in outer diameter, as well as porous disks, were ordered from Zircar Zirconia of Florida, New York, U.S.A. They are stated by the manufacturer to contain approximately 88–89 wt% ZrO_2, 10 wt% Y_2O_3 and 1–2 wt% HfO_2, along with trace oxide concentrations of approximately 0.12 wt% SiO_2, 0.14 wt% TiO_2, 0.09 wt% CaO, 0.04 wt% Fe_2O_3, 0.03 wt% MgO and less than or equal to 0.01 wt% of Al_2O_3, Na_2O, SnO_2, Cr_2O_3 and Ag_2O. Impurities in the zirconia, especially Cr, Sn, Si, K and Na, must be monitored as possible poisons for nickel catalysts in SOFCs. The exceptionally high porosity of the material, stated as 76% by the manufacturer, is achieved using matted YSZ fibers rather than conventional sintered YSZ crystallites, which typically achieve maximum porosities of near 40% while maintaining mechanical stability.

Beds are formed, containing approximately 6.5–11.5 g of perovskite catalyst granules, in the hot zone of the porous YSZ tubes and have a volume of approximately 5.7–14.5 cm^3, a cylindrical height of approximately 2.0–3.8 cm and a void fraction typically of 0.3. Four layers of platinum–rhodium gauze, separated by 3.2 mm (0.12 in.) thick porous YSZ disks, were used as a base-line catalyst for comparison of activities of the perovskite catalysts. The Pt90–Rh10 (wt%) wire gauze was purchased from Alfa Aesar and has approximately 31 openings per linear centimeter (80 mesh) and a wire diameter of 0.076 mm.

Air is fed into the reactor from an in-house compressed air supply through a Model 1179A MKS mass flow controller, which is calibrated for flow rates of up to 5000 sccm (standard cubic centimeters per minute). Air flows into the lumen between the inner and outer reactor tubes (see Fig. 4) and permeates through the walls of the porous YSZ tube.

Reactor exhaust flows through traps to minimize water in gas chromatography columns. Exhaust gas samples of 0.25 mL are injected manually by syringe into a gas chromatography sample port. Exhaust gas is analyzed for H_2, CO, CO_2, CH_4 and N_2 with a Shimadzu GC-14A gas chromatograph with a thermal conductivity detector and a stainless steel column, 1.8 m (6 foot) × 0.3 cm (0.12 in.), containing an Alltech Carbosphere

80/100 adsorbent. To calibrate the gas chromatography apparatus, specialty gas mixtures containing known concentrations of H_2, CO, CO_2, CH_4 and N_2 over a range of concentrations near that of the ideal partial oxidation product distribution of diesel fuel of 23.25% H_2 and 26.01% CO were purchased from Airgas Corporation. Exhaust flow rate is measured at ambient temperature and pressure using a 100 mL bubble flow meter, and the measured flow rate is corrected to standard temperature and pressure.

2.2. Experimental method

Diesel fuel reforming studies and tests of new catalysts were typically performed on a 4-day cycle for each catalyst. To demonstrate acceptable oxidation activity for new catalyst compositions, catalysts were tested in an approximately 10% excess of oxygen from air on the first day to prove ability for complete oxidation of diesel fuel into CO_2 and water. Diesel fuel flow rates were between approximately 0.06 and 0.07 g min^{-1}. To allow partial oxidation and production of H_2 and CO, air flow on the second day was decreased incrementally by 50 sccm every 40 min while fuel flow rate was kept constant. Air flow rate ranged from an initial 810 to approximately 250 mL min^{-1}. Flow rate and concentration measurements were taken every 10 min for 7 h. Steady-state partial oxidation was continued throughout the third and fourth days. Diesel fuel was fed to the reactor for approximately 7 h each day, resulting in a total of 28 h of reforming time for each catalyst. Space velocities ranged from 60,000 to 120,000 h^{-1}. The temperature was maintained at 950 °C at the thermocouple in the exhaust, 1 cm below the catalyst bed. All studies were conducted at ambient pressure (typically near 78 kPa (0.77 atm) in Boulder, Colorado, U.S.A). Mass balance of carbon is calculated from the calibrated volume flow rate of liquid diesel fuel entering the system, the measured density of the liquid fuel, the H:C atomic ratio determined by certified analytical laboratories, and the total carbon in the exhaust contained in the CO, CO_2 and CH_4 measured by gas chromatography. As a control to verify the efficacy of the porous zirconia tubes, dense alumina tubes were substituted in the region over which fuel is heated from 300 to 950 °C. This resulted in rapid deposition of carbon.

2.3. Analysis of diesel fuel

Diesel fuel was purchased from automotive pumps of commercial fueling stations in Boulder County, Colorado, U.S.A. For the work discussed, fuel was purchased in May 2007. Fuel was labeled at the pump as containing a maximum of 15 ppm by mass sulfur. Samples were analyzed for sulfur, carbon, hydrogen and nitrogen content by three independent and certified analytical laboratories: Intertek Caleb Brett of Chicago, Illinois, Wyoming Analytical Laboratories at Golden, Colorado, U.S.A. and Galbraith Laboratories of Knoxville, Tennessee, U.S.A. Intertek Caleb Brett and Wyoming Analytical Laboratories used ASTM Standard D5453 to measure sulfur content and Intertek Caleb Brett and Galbraith used ASTM Standard D5291 to measure content of carbon, hydrogen and nitrogen.

Sulfur content was determined by Wyoming Analytical Laboratories to be 7 ppm by mass and by Intertek Caleb Brett to be 9 ppm by mass, in reasonable agreement and meeting the 15 ppmw sulfur limit. Intertek Caleb Brett reported carbon content as 86.91 wt%, hydrogen 13.06 wt% and nitrogen <0.75 wt% yielding a hydrogen-to-carbon atomic ratio of 1.79–1. Analysis by Galbraith Laboratories determined the fuel to have an atomic ratio of H:C of 1.83:1. A batch of diesel fuel analyzed by Galbraith Laboratories in September, 2005 (before ultra-low sulfur regulations were introduced) was determined to have an atomic ratio of H:C of 1.78:1, and a sample purchased prior to 2004, upon which the thermodynamic calculations of Fig. 2 are based, had an atomic ratio of 1.86:1. Earlier samples contained <500 ppm by mass sulfur according to the Galbraith analysis.

2.4. Preparation of catalysts

The diesel fuel reforming catalysts, $La_{0.5}Sr_{0.5}CoO_{3-\delta}$ and $La_{0.5}Sr_{0.5}FeO_{3-\delta}$, were both synthesized at Eltron Research using standard techniques of solid-state chemistry [6,21]. Each catalyst is formed from oxides (La_2O_3, Fe_2O_3 and Co_3O_4) and carbonates ($SrCO_3$) weighed to give the desired perovskite stoichiometry. The starting materials are high-purity (99% by mass minimum), reagent-grade chemicals purchased from Sigma–Aldrich Inc. of Milwaukee, Wisconsin, U.S.A. and Alfa Aesar. Because some of the reagents form hydrates or contain variable quantities of water, which may lead to discrepancies in mass and thus to deviations from the desired perovskite stoichiometry, water content is determined for each starting material by thermogravimetric analysis (TGA) using a Shimadzu model TGA-50 thermogravimetric analyzer. Using the corrections for water content, the starting materials are weighed to obtain the desired calculated dry masses to yield the desired perovskite stoichiometry and are combined in a wide-mouth 250 mL polypropylene Nalgene bottle. Twenty zirconia ball-milling cylinders (1 cm in diameter and 1 cm in height) are added to the power, and the bottle is filled with 2-propanol. The closed bottle is placed onto a ball mill, and the starting materials are thoroughly mixed overnight and then transferred to a Pyrex drying dish. Upon evaporation of the 2-propanol, the material is sifted through number 45 and 170 sieves and placed into alumina crucibles which are heated at a rate of 3 °C/min in air in an electric furnace to 1200 °C and held at temperature for 12 h to synthesize $La_{0.5}Sr_{0.5}CoO_{3-\delta}$ and $La_{0.5}Sr_{0.5}FeO_{3-\delta}$.

Upon cooling, the perovskite materials are sifted through number 45 and 170 sieves. Physical grinding via mortar and pestle is occasionally necessary to break up agglomerates that form during the first calcining process. Once sifted, the materials are analyzed using powder X-ray diffraction (XRD) and compared to standard reference patterns to verify that the desired perovskite crystalline structure has formed and to demonstrate the absence of starting materials or undesired solid-state side-products. If necessary, the material is re-ground and re-mixed, and a second calcination is performed (typically

at 1200 °C for $La_{0.5}Sr_{0.5}CoO_{3-\delta}$ and at 1250 °C for $La_{0.5}Sr_{0.5}FeO_{3-\delta}$) until X-ray diffraction has verified that the desired perovskite crystal structure has formed. In order to generate a desired particle size distribution, the synthesized material is placed in an attrition mill with zirconia attrition media and 2-propanol for 4 h at 400 rpm. The material is dried and sifted through number 45 and 170 sieves.

Porous catalyst granules are then formed from the powdered perovskite material. The perovskite powder is mixed with a pore former (ARGO 100% pure cornstarch) and a binder (Butvar B-79 polyvinyl butyral) in a 100:60:10 w/w/w ratio, respectively. This is placed in a 250 mL wide-mouth polypropylene Nalgene bottle filled with acetone and ball milled for several hours in order to thoroughly mix. The mixture is then transferred to a Pyrex drying dish to evaporate the acetone. Constant agitation is applied to the mixture through the drying process to limit the formation of large clumps. Once dry, the mixture is sifted through number 45 and 170 sieves. The dry powder is then cold-pressed in a 5.72 cm (2.25 in.) diameter pellet die at 1379 bar (20,000 psi). The pressed pellets are removed and placed onto alumina plates and are heated in air in an electric furnace at a rate of 0.5 °C/min from room temperature to 450 °C to burn out the cornstarch and binder to form pores. The $La_{0.5}Sr_{0.5}CoO_{3-\delta}$ material is then heated to 1150 °C and sintered for 4 h in air and the $La_{0.5}Sr_{0.5}FeO_{3-\delta}$ sintered at 1200 °C. Upon cooling, the porous pellets are broken into granules using a mortar and pestle and sized between number 8 and 12 sieves. The granules are then used to form catalyst beds in the hot zones of the porous membrane reactors.

2.5. Powder X-ray diffraction

Powder X-ray diffraction data is gathered using a Philips X-ray powder diffractometer equipped with a Model 1830 X-ray generator, a Model 1050 goniometer, and a Model PW 3710 control unit. Philips X'pert® diffraction software is used to control the instrument and analyze the data. The X-ray beam is generated from a copper source and passes through a fixed 1° divergent slit, a 0.04° Soller slit, a fixed 2 mm receiving slit and second 0.04° Soller slit. Both the divergent and receiving slits can be varied to adjust the resolution and intensity as required. The initial beam contains both Cu Kα1 and Cu Kα2 X-rays. At low diffraction angles, the resolution of the instrument is insufficient to resolve the splitting that results from the multiple-energy X-ray beam. However, peak splitting is resolved at higher diffraction angles—typically those above a 2θ angle of 50°. According to Azároff and Buerger [22], most X-ray measurement errors vanish as θ approaches 90° according to the Bragg relation, $n\lambda = 2d \sin\theta$, and X-ray wavelengths are known to better than 1 part in 100,000. X-ray data is reported to the number of significant figures, consistent with American Crystallographic Association standards [23].

An aluminum plate, machined with a shallow reservoir approximately 1 mm deep, is used to hold and position the powder samples within the X-ray diffractometer. An optically flat glass microscope slide is used to level the powdered material with the upper surface of the aluminum plate and to pack the powder. Variations in the position of the sample and sample holder can produce slight shifts in the X-ray diffraction peaks. The software allows X-ray diffraction data to be compared to an extensive database of reference patterns, including those made available through the International Center for Diffraction Data (ICDD).

2.6. Scanning electron microscopy and energy dispersive X-ray spectroscopy

Catalyst morphology is characterized using a JEOL JSM 5610 scanning electron microscope. The electron beam is produced from a conventional resistively heated tungsten tip, and beam voltage can be varied between 500 and 30,000 V. For bulk elemental analysis, the microscope is equipped with a Princeton Gamma-Tech energy-dispersive X-ray spectrometer using a liquid-nitrogen cooled, Si(Li) X-ray detector and an Avalon 8000 analysis package which automatically approximates and subtracts bremsstrahlung radiation. Low-Z elements, including carbon, nitrogen and oxygen, can be detected to some extent. However, carbon in samples remains difficult to quantify because of carbon contamination which can arise from adsorption and electron-beam cracking of hydrocarbon pump oils from the relatively modest vacuum of the microscope chamber of about 1.0×10^{-5} Torr (1.3×10^{-3} Pa), generated by a rotary-vane rough pump and an oil diffusion pump.

2.7. Surface area analysis

Surface area analysis of the catalysts is preformed using Brunauer–Emmett–Teller (BET) physical adsorption methods [24] using a Quantachrome Nova 2000e surface area analyzer/porosimeter. Nitrogen, N_2, is used as the probe molecule.

3. Results and discussion

3.1. Studies on total oxidation of diesel fuel

Fig. 8 shows results for the complete dry oxidation of diesel fuel using (a) stacked platinum–rhodium gauze separated by disks of porous YSZ and (b) a bed of granules of $La_{0.5}Sr_{0.5}CoO_{3-\delta}$. A tube furnace provided external heating to 950 °C. However, temperatures at the surface of the catalysts are likely greater, due to the exothermic oxidation reactions. Oxygen in air was added 10% in excess of the stoichiometry required for complete conversion to CO_2 and H_2O. Catalysts showing high activity for complete combustion of diesel fuel might find application for oxidation of hydrocarbons and CO in diesel-automotive pollution control devices. Complete oxidation of diesel fuel, and the heat generated, may also be useful for heating large SOFC stacks during start-up.

The dotted lines in Fig. 8a and b indicate the production of CO_2 calculated from the mass of carbon entering the system in the diesel fuel and assuming complete combustion to CO_2 and H_2O. Mass of carbon entering the system in diesel fuel was 0.062 and 0.060 g min^{-1}, respectively. Activity of both

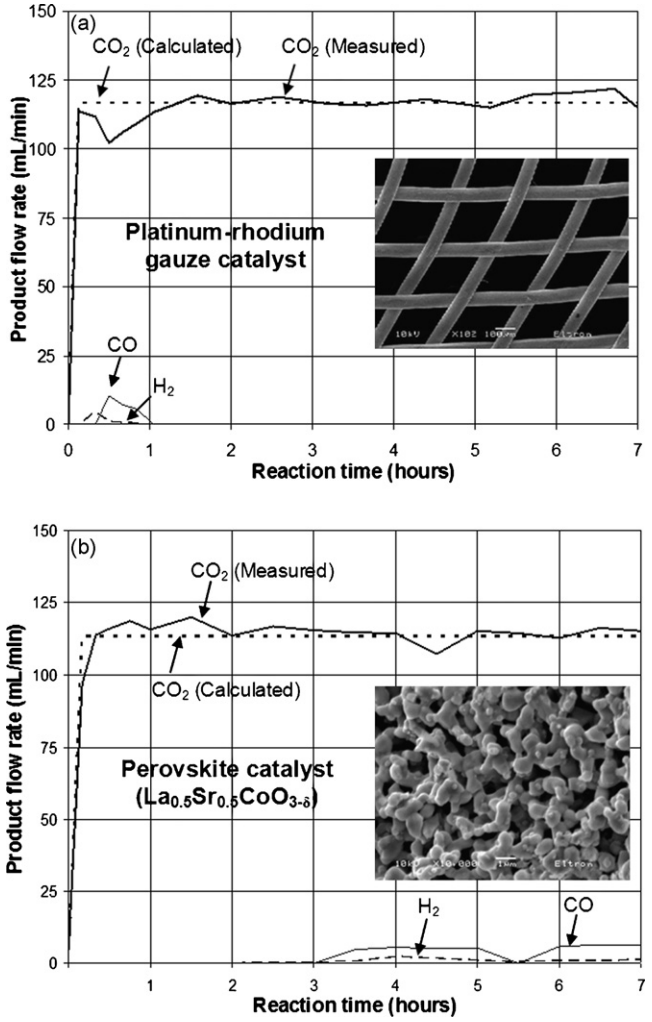

Fig. 8. Results for complete dry oxidation of pump-grade diesel fuel into $CO_2 + H_2O$ at >950 °C. (a) Pt–Rh wire gauze. (b) $La_{0.5}Sr_{0.5}CoO_{3-\delta}$.

catalysts shown (albeit with external heating) was sufficient for complete combustion of the fuel. The carbon mass balance was within experimental error. Iron-based perovskites show similar activity for complete combustion. It is concluded that perovskite catalysts can be as active as noble metals in the case of complete oxidation. This is in accord with reports by Libby (Nobel Prize in Chemistry, 1960), who drew similar conclusions [25,26]. As is discussed below, lattice constants of cobalt and iron-based perovskites are similar to that of noble metals [23], which may, in part, be responsible for the similarity. According to Nakamura et al. [27], the parent compound, $LaCoO_3$, requires a partial pressure of oxygen of at least 1×10^{-7} bar at 1000 °C to remain stable. The parent iron compound, $LaFeO_3$, is much more stable, decomposing to La_2O_3 and Fe at 1000 °C only when the partial pressure of oxygen drops below 1×10^{-17} bar. In general, perovskites remain stable under oxidizing conditions, but some may decompose under strongly reducing conditions.

Platinum–rhodium gauze was used as an ideal catalyst and as a basis for comparison of the activity of the perovskite catalysts. Platinum–rhodium wire gauze is known to adsorb and dissociate

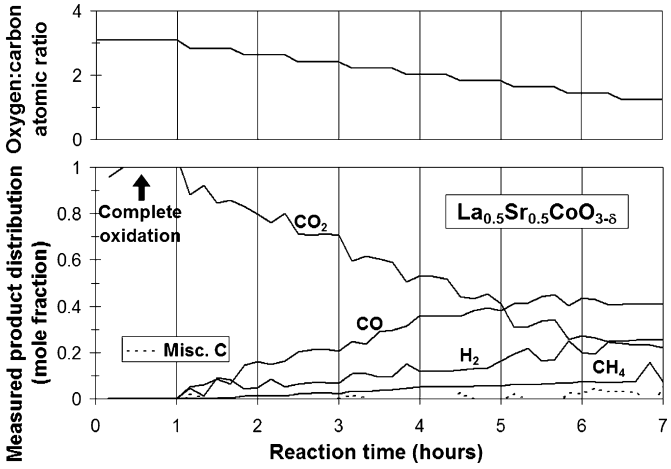

Fig. 9. Partial oxidation of diesel fuel using $La_{0.5}Sr_{0.5}CoO_{3-\delta}$.

molecular oxygen, forming highly active adsorbed oxygen atoms. Highly active and mobile oxygen adatoms on Pt–Rh are desired to oxidize the more stable aromatic compounds in diesel fuel. The perovskite surfaces presumably also provide a highly active dissociated form of oxygen and catalyze complete oxidation of the aromatic compounds in excess oxygen.

3.2. Partial oxidation of diesel fuel

After demonstrating sufficient activity for complete combustion, which produced CO_2 at a rate of approximately 5.0×10^{-2} mol min^{-1}, and water at an estimated rate of 3.5×10^{-2} mol min^{-1}, air flow was reduced, while flow of diesel fuel and reformer temperature were held constant. Figs. 9 and 10 show results for catalysts of $La_{0.5}Sr_{0.5}CoO_{3-\delta}$ and $La_{0.5}Sr_{0.5}FeO_{3-\delta}$, respectively, starting with slight excess oxygen. As air flow is decreased and as conditions become more reducing, production of CO_2 decreases and concentrations of CO, H_2 and CH_4 simultaneously increase. The corresponding oxygen-to-carbon atomic ratios are plotted above. An oxygen-to-carbon atomic ratio of 2.895:1 corresponds to the stoichiometric ratio required for complete

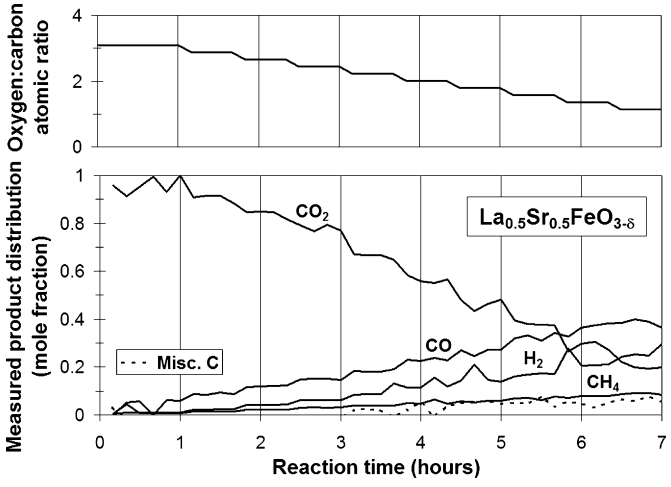

Fig. 10. Partial oxidation of diesel fuel using $La_{0.5}Sr_{0.5}FeO_{3-\delta}$.

oxidation of diesel fuel by the reaction: $H_{1.79}C + 1.448\ O_2 = 0.895\ H_2O + CO_2$ for fuel empirically analyzed by Intertek Caleb Brett to contain an atomic ratio of hydrogen-to-carbon of 1.79:1. An oxygen-to-carbon atomic ratio of 1:1 is required to theoretically maximize production of synthesis gas according to the partial oxidation reaction: $H_{1.79}C + 0.5\ O_2 = 0.895\ H_2 + CO$.

Plotted as dashed lines at the bottoms of Figs. 9 and 10 is miscellaneous carbon, which includes all carbonaceous components other than CO, CO_2 and CH_4 that were not detected by gas chromatography. Miscellaneous carbon could include small, undetected molecules such as ethane, unreacted diesel fuel such as naphthalene or soot. Miscellaneous carbon is calculated from the lack of closure in the mass balance, determined from the difference in carbon flowing into the system as diesel fuel and exiting as CO, CO_2 and CH_4. Although some carbonaceous material has escaped reforming, the quantity is small, and beds of catalysts in the reactor were by no means optimized.

Comparing the calculated values in Fig. 2, which predicted complete conversion to H_2 + CO above 950 °C, to the measured values in Figs. 9 and 10, it is seen that considerable CO_2 and CH_4 were produced. This implies that the system was either not brought to equilibrium in the hot zone of the reactor or that the undesired products, CO_2, CH_4 and also H_2O formed in the cooler lines of the exhaust. Again the system was by no means optimized, and exhaust lines of alumina and stainless steel are likely not catalytically inert and will need to be replaced.

Table 1 summarizes the detected product distributions produced with beds of $La_{0.5}Sr_{0.5}CoO_{3-\delta}$ and $La_{0.5}Sr_{0.5}FeO_{3-\delta}$ in the hot zone at maximum syngas production and minimum oxygen entering the reactor. Considerable undesired CO_2, CH_4 and H_2O have formed in the unoptimized system. Tables 2 and 3 list the percent of carbon and hydrogen in the original fuel which have appeared in the various products. Optimization, which might include simple increase in the size of catalyst bed in the hot zone to ensure equilibrium as well as a change of components in the exhaust lines, needs to be performed.

Table 1
Molar composition of product stream at maximum syngas production

	$La_{0.5}Sr_{0.5}CoO_{3-\delta}$ (%)	$La_{0.5}Sr_{0.5}FeO_{3-\delta}$ (%)
H_2	20.7	23.3
CO	33.2	28.8
CO_2	18.1	15.5
CH_4	6.0	6.8
H_2O*	22.0	25.6

*Assuming all hydrogen not accounted for in the mass balance reacts to form H_2O.

Table 2
Mole percent of feed carbon reacting to form CO, CO_2 and CH_4 at maximum syngas production

	$La_{0.5}Sr_{0.5}CoO_{3-\delta}$ (%)	$La_{0.5}Sr_{0.5}FeO_{3-\delta}$ (%)
CO	54.4	51.9
CO_2	29.7	28.0
CH_4	9.8	12.2
Closure*	6.1	7.9

* refers to miscellaneous carbon products not detected by gas chromatography.

Table 3
Mole percent of feed hydrogen reacting to form H_2 and CH_4 at maximum syngas production

	$La_{0.5}Sr_{0.5}CoO_{3-\delta}$ (%)	$La_{0.5}Sr_{0.5}FeO_{3-\delta}$ (%)
H_2	37.8	47.0
CH_4	21.9	27.3
Closure*	40.3	25.7

* refers to miscellaneous hydrogen products (likely mostly water) that were not detected by gas chromatography.

After each set of experiments (28 h total), the reformer was disassembled to check for carbon deposits. The catalyst bed in the hot zone and inner walls of the porous YSZ tube showed minimal or no visual accumulation of carbon. The control, which used a dense alumina tube in place of the porous YSZ tube, showed significant carbon build-up on the inner walls after *only* 20 min of reaction. This confirms that effusing air through the porous zirconia wall suppresses carbon formation on its inner surfaces.

The small (0.635 mm diameter) opening of the stainless steel fuel feed tube is a potential location for carbon accumulation that could plug the reformer. Infrared radiation from the catalyst hot zone as well as convection currents could heat the stainless steel tube above the cracking temperature of the least stable hydrocarbons in the fuel. There was some accumulation of tar and solid carbon on the outer surface of the tube. Future work will examine deposition of silver onto the stainless steel feed tube to help oxidize deposited carbon and to reflect infrared radiation. Silver is an excellent oxidation catalyst and, furthermore, has the highest permeability for oxygen of any common metal [28]. Silver thus can provide a source of oxygen diffusing to the surface from beneath to oxidize adsorbed carbon. Silver also has the highest reflectivity for infrared radiation of any common metal.

3.3. Surface area analysis results

The BET surface area analysis indicated that the $La_{0.5}Sr_{0.5}CoO_{3-\delta}$ and $La_{0.5}Sr_{0.5}FeO_{3-\delta}$ catalyst granules, as synthesized, had specific surface areas of 0.39 and 0.51 $m^2\ g^{-1}$, respectively. The surface areas are low relative to most catalysts and are near the limits of measurement of the in-house BET apparatus. No attempts were made to improve surface area during synthesis because of losses by sintering predicted if the catalysts are used near 1000 °C for extended times. After 28 h of use in the reactor, the surface area of the $La_{0.5}Sr_{0.5}CoO_{3-\delta}$ actually increased to 1.6 $m^2\ g^{-1}$ due to etching, as discussed below. The surface area of the $La_{0.5}Sr_{0.5}FeO_{3-\delta}$ decreased slightly after use.

3.4. X-ray diffraction analysis of the perovskite catalysts

Figs. 11 and 12 show X-ray diffraction patterns of $La_{0.5}Sr_{0.5}CoO_{3-\delta}$ and $La_{0.5}Sr_{0.5}FeO_{3-\delta}$, respectively, both

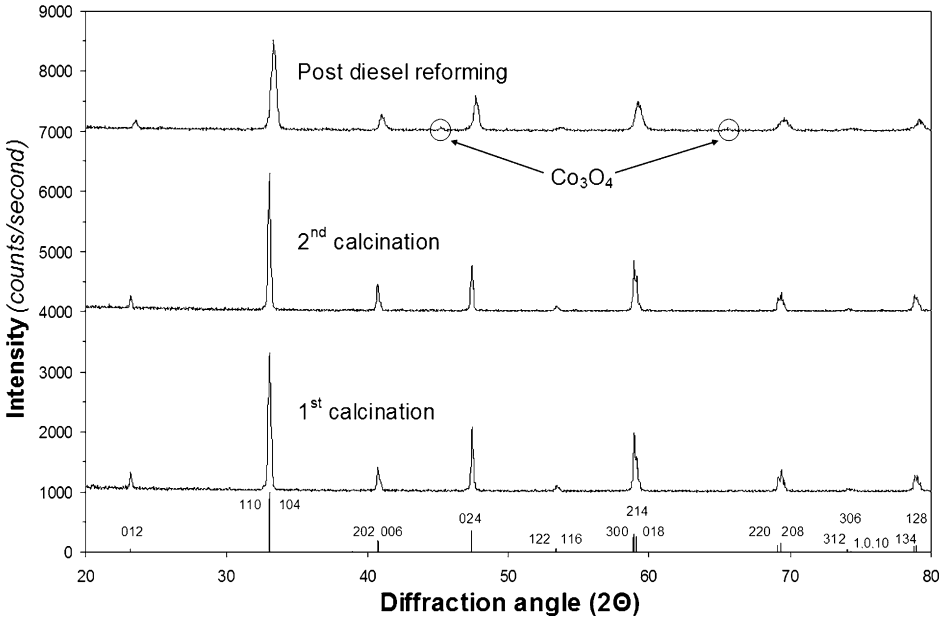

Fig. 11. X-ray diffraction of $La_{0.5}Sr_{0.5}CoO_{3-\delta}$ catalyst before and after use. Some slight decomposition has occurred.

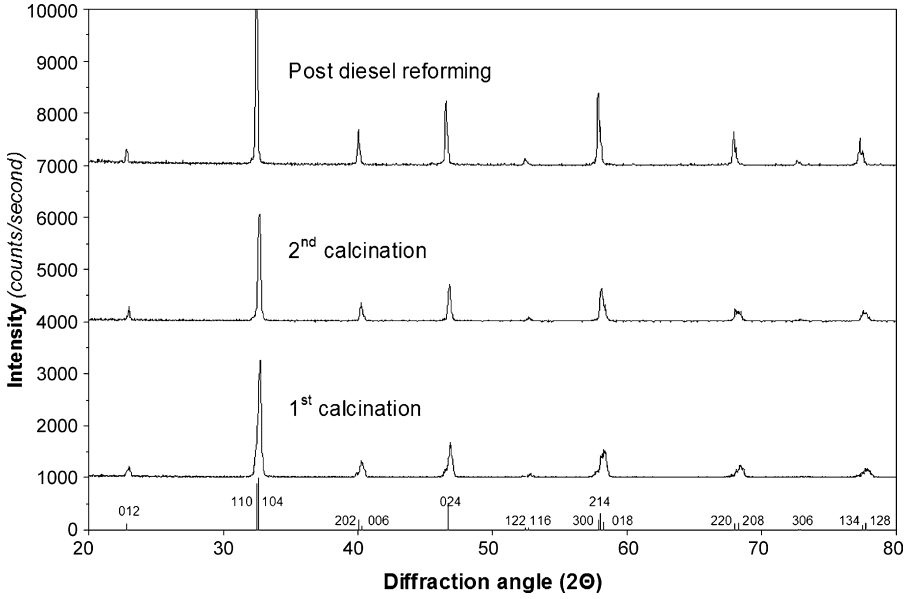

Fig. 12. X-ray diffraction of $La_{0.5}Sr_{0.5}FeO_{3-\delta}$ catalyst before and after use. The iron-based perovskite is stable under the reaction conditions employed.

before and after use in the reactor. Table 4 summarizes lattice parameters of $La_{0.5}Sr_{0.5}CoO_{3-\delta}$ and $La_{0.5}Sr_{0.5}FeO_{3-\delta}$ as synthesized and after use, along with reference diffraction data [29–31]. Symmetry assignment of both is rhombohedral (slightly distorted from the ideal cubic perovskite crystal structure).

A comparison of the diffraction data of $La_{0.5}Sr_{0.5}CoO_{3-\delta}$ (Fig. 11) indicates a slight broadening of peaks after use of the catalyst in the reactor. The X-ray line broadening suggests that the mean particle size may have been reduced during the reforming experiments. This is supported by scanning electron microscopy images (see below) showing etching of the $La_{0.5}Sr_{0.5}CoO_{3-\delta}$ samples and BET surface analysis, which

Table 4
Reference and measured lattice parameters for $La_{0.5}Sr_{0.5}CoO_{3-\delta}$ and $La_{0.5}Sr_{0.5}FeO_{3-\delta}$ catalysts used before and after diesel reforming experiments

Material	a (Å)	c (Å)	Volume (Å^3)
$La_{0.5}Sr_{0.5}CoO_{3-\delta}$ [29]	5.4300(3)	13.2516(1)	338.38
$La_{0.5}Sr_{0.5}CoO_{3-\delta}$ (as synthesized)	5.432(3)	13.253(8)	338.6(1)
$La_{0.5}Sr_{0.5}CoO_{3-\delta}$ (postdiesel-reforming)	5.435(6)	13.23(1)	338(1)
$La_{0.5}Sr_{0.5}FeO_{3-\delta}$ [30,31]	5.51107(1)	13.41578(2)	352.87
$La_{0.5}Sr_{0.5}FeO_{3-\delta}$ (as synthesized)	5.505(2)	13.443(4)	352.9(2)
$La_{0.5}Sr_{0.5}FeO_{3-\delta}$ (postdiesel-reforming)	5.518(1)	13.450(6)	354.7(1)

All specimens display rhombohedral symmetry.

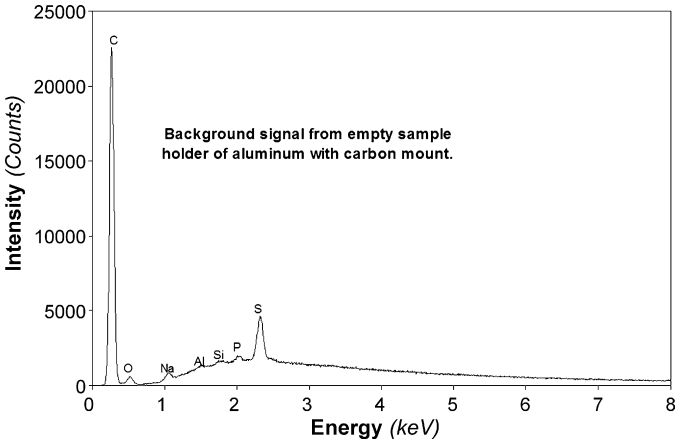

Fig. 13. EDS spectrum of a sample holder (aluminum stub with carbon mount) used as a control to show background peaks. Note the large carbon signal from the carbon mount.

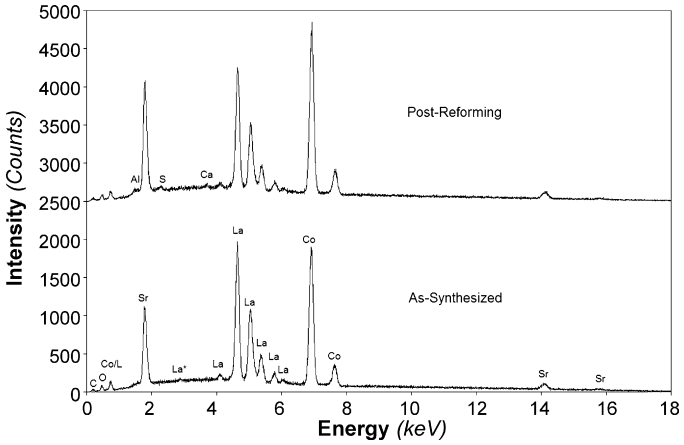

Fig. 14. EDS of an as-synthesized $La_{0.5}Sr_{0.5}CoO_{3-\delta}$ catalyst (lower) compared to same catalyst after 1 week of use in the reactor at 950 °C (upper). The catalyst has remained carbon-free.

shows an increase in surface area of the $La_{0.5}Sr_{0.5}CoO_{3-\delta}$ catalyst after use. Two new minor peaks also appear after use in the reactor and are assigned to Co_3O_4, based upon comparison to standard libraries of X-ray data [32]. However, possible assignments to other compounds cannot be ruled out. The diffraction information implies that the cobalt-based perovskite catalysts are not completely stable under the reducing conditions encountered in these experiments. More stable formulations, such as $La_{0.8}Sr_{0.2}CoO_{3-\delta}$ may need to be investigated.

A comparison of the X-ray diffraction data of $La_{0.5}Sr_{0.5}FeO_{3-\delta}$ (Fig. 12), before and after use in the reactor, shows little significant change. Calculated unit cell parameters for the $La_{0.5}Sr_{0.5}FeO_{3-\delta}$ catalyst agreed well with the references published by Dann et al. [30,31].

3.5. X-ray spectroscopy and scanning electron microscopy analysis

Energy dispersive (X-ray) spectroscopy (EDS) data was collected from both the $La_{0.5}Sr_{0.5}CoO_{3-\delta}$ and $La_{0.5}Sr_{0.5}FeO_{3-\delta}$ samples before and after use in the reactor. As a control to account for background X-ray fluorescence from the mostly aluminum microscope chamber, an aluminum sample holder with carbon mount, and the housing of the X-ray detector, a spectrum was taken from the empty sample holder and is shown in Fig. 13. The background spectrum shows typical peaks arising from carbon, oxygen, sodium, aluminum, silicon, phosphorus and sulfur.

Fig. 14 shows EDS spectra obtained from the $La_{0.5}Sr_{0.5}CoO_{3-\delta}$ catalyst before and after use in the reactor. Small signals from aluminum, sulfur and calcium appear in the catalysts after use in the reactor (upper spectrum) but do not appear in the spectrum of the catalysts before use. The aluminum and sulfur signals could arise from the background of the chamber and sample holder (see Fig. 13) if the angles of the incident electron beam and emerging X-ray beams varied between catalysts granules, which can easily occur. However, the reactor did contain alumina tubes, and catalysts were prepared using alumina crucibles. Sulfur could have accumulated from exposure to the diesel fuel, although background signals cannot be ruled out (see Fig. 13). Although bulk sulfides of cobalt were predicted to be unstable (see Fig. 5), sulfides of both lanthanum (La_2S_3) and strontium (SrS) are fairly stable, with melting points of >2100 and >2000 °C, respectively. Sulfur could be bound to both La and Sr. Sulfur could also be strongly bound to calcium as CaS. The calcium signal in Fig. 14 could arise from the reactor components or from the diesel fuel, although the strontium carbonate used to synthesize the perovskite typically contains calcium as a minor impurity. It might be noted that calcium hydroxide is injected into power-plant smoke stacks to remove sulfur because of the strong affinity of calcium for sulfur (see Fig. 5).

Phosphorus is a known poison for many noble metal catalysts [33] because of the refractory phosphide compounds [34] formed (for example, PtP_2 mp ca 1500 °C). Cobalt forms the phosphide, Co_2P, which melts at 1386 °C, and phosphorus is expected to poison cobalt catalysts. Compounds of phosphorus have been added to automotive engine lubricants to form brittle iron phosphides which act as high-temperature anti-seize lubricants between pistons and cylinders. There is no clear evidence for bulk phosphide formation. Silicon, another possible contaminant, is difficult to observe by EDS, because the main silicon peaks overlap with the strong strontium peak (actually several closely spaced unresolved strontium peaks) below 2 keV. Comparison of Fig. 13 with Fig. 14 shows that no significant bulk carbon has accumulated on the $La_{0.5}Sr_{0.5}CoO_{3-\delta}$ used in the hot zone, in agreement with calculations of Fig. 2. The small carbon peaks seen in Fig. 14 are attributed to cracking of residual pump oil in the SEM chamber by the electron beam.

Fig. 15 shows EDS spectra for the $La_{0.5}Sr_{0.5}FeO_{3-\delta}$ catalyst as synthesized (lower) and after use in the reactor (upper). The small aluminum signals seen in both spectra are assigned to the background. No obvious bulk impurities, including carbon, have accumulated on the $La_{0.5}Sr_{0.5}FeO_{3-\delta}$ catalyst after use. Phosphorus was sought because of possible formation of Fe_2P (melting point 1100 °C), which could poison iron catalysts, but no evidence for P was seen. No bulk sulfur or calcium was

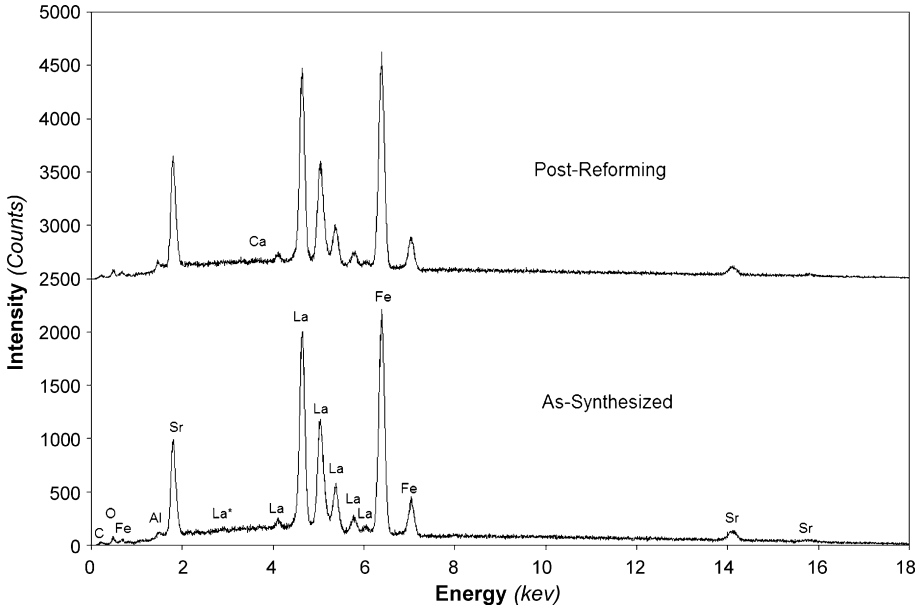

Fig. 15. EDS of an as-synthesized $La_{0.5}Sr_{0.5}FeO_{3-\delta}$ catalyst (lower) compared to same catalyst after 1 week of use in the reactor at 950 °C (upper). Catalyst is carbon free and has not formed a bulk sulfide.

detected on the iron-based perovskite. It should be noted, however, that EDS is not surface sensitive, and monolayers of potential catalyst poisons adsorbed from the diesel fuel and reactor would not be detected.

The Pt–Rh wire-gauze was also analyzed by EDS for S, P, Si and other potential catalyst poisons. There was no bulk formation of these elements detected.

Fig. 16a and b shows SEM images of $La_{0.5}Sr_{0.5}CoO_{3-\delta}$ before and after use in the reactor, respectively. Fig. 16c and d shows corresponding images for $La_{0.5}Sr_{0.5}FeO_{3-\delta}$. Fig. 16b shows that the $La_{0.5}Sr_{0.5}CoO_{3-\delta}$ has been etched after exposure to reactor conditions. This is consistent with X-ray line broadening and BET surface area measurements. The $La_{0.5}Sr_{0.5}FeO_{3-\delta}$ sample of Fig. 16d shows some sintering after use in the reactor.

3.6. Discussion-perovskite catalysts

Oxides with the perovskite crystal structure have been used as catalysts in fuel cells and for other applications since at least

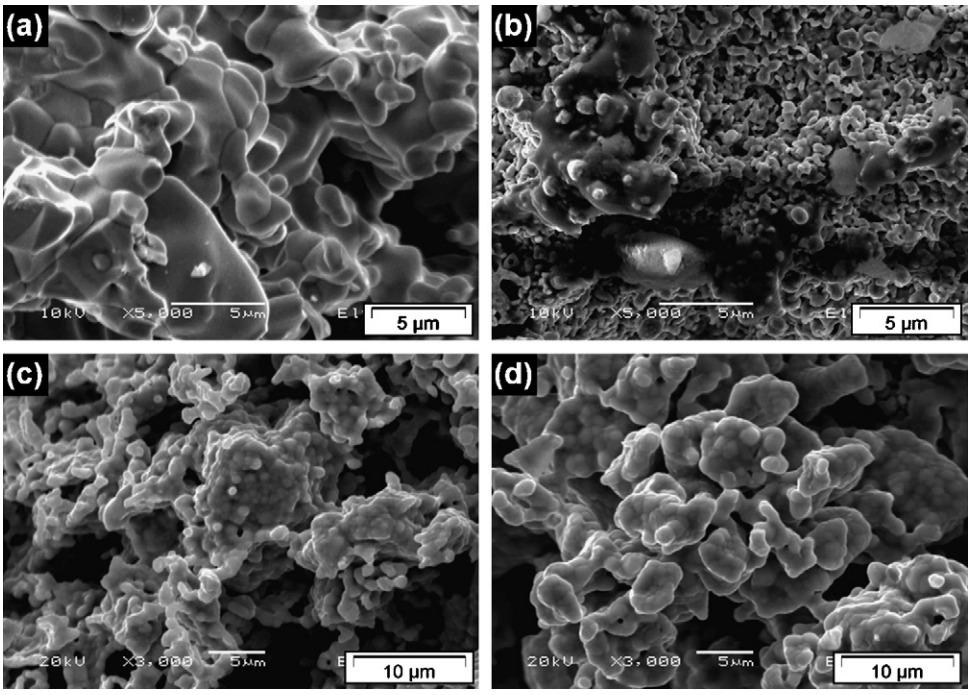

Fig. 16. SEM images of perovskite catalysts before and after use in the reactor. (a) $La_{0.5}Sr_{0.5}CoO_{3-\delta}$ as synthesized. (b) $La_{0.5}Sr_{0.5}CoO_{3-\delta}$ after use in the reactor showing pronounced etching. (c) $La_{0.5}Sr_{0.5}FeO_{3-\delta}$ as synthesized. (d) $La_{0.5}Sr_{0.5}FeO_{3-\delta}$ after use in reactor showing some sintering.

Table 5
Lattice constants of face-centered cubic noble metals showing similarity to lattice constants of perovskites [23]

Element	Lattice constant (Å)
Rh	3.8044(1)
Ir	3.8389(5)
Pd	3.8902(3)
Pt	3.9237(3)
$LaCoO_3$	3.82(1)
$LaCrO_3$	3.88
$LaFeO_3$	3.89–3.899
$LaMnO_3$	3.88–3.90

the 1950s [6,35]. The lattice constants of cubic perovskites are similar to that of noble metals [23] (see Table 5), which, in part, may be responsible for similar catalytic activity. The tetragonal and rhombohedral distortions which perovskites undergo [6] are only slight deviations from cubic symmetry, and reported rhombohedral lattice constants, such as those listed in Table 4, can obscure the similarities in lattice constants.

It is very well established from work on fuel cell and oxygen transport membranes [36–38] that materials such as $La_{0.5}Sr_{0.5}CoO_{3-\delta}$, $La_{0.5}Sr_{0.5}FeO_{3-\delta}$, and related perovskite compounds readily adsorb and dissociate molecular oxygen by the reaction: $O_2 + 4e^- = 2O^{2-}$ and allow oxygen anions, O^{2-}, to rapidly diffuse through the bulk lattice. Stoichiometric parent compounds such as $LaCoO_3$ and $LaFeO_3$ are doped with Ca^{2+} and Sr^{2+} to replace La^{3+}. For every two La^{3+} ions which are replaced, one less O^{2-} ion is required in the lattice for charge neutrality and thus a vacancy is created (see Fig. 17). The vacancies allow oxygen anions to hop between neighboring oxygen-anion sites in the perovskite lattice (see Fig. 1).

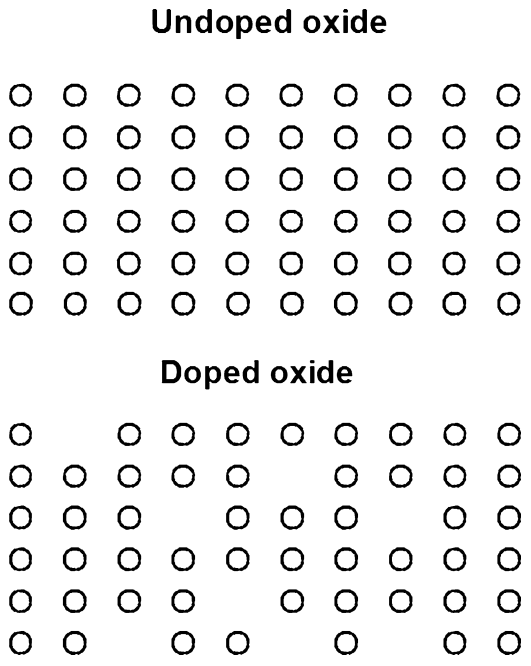

Fig. 17. Schematic representing creation of vacancies in oxide lattices to enhance mobility of oxygen. Mobile oxygen is desirable in oxidation catalysts, catalyst supports, oxygen transport membranes and self-cleaning reactor walls to allow oxidization of carbon from beneath.

This is analogous to the doping of ZrO_2 with Y^{3+} or Ca^{2+} to replace Zr^{4+} and to create oxygen-anion vacancies and thus high oxygen mobility in zirconia solid-state electrolytes. According to Smith [19], this was realized already by 1943 by Wagner. Doping of CeO_2 and replacing Ce^{4+} with ions of lower formal charge such as La^{3+} or Gd^{3+} in CGO likewise enhances oxygen transport in cerates used in oxidation catalysts, solid-state electrolytes, heating mantels, and self-cleaning oven walls. In general, oxygen-anion mobility in the catalytic perovskites and membranes is substantially greater than in YSZ and CGO [37]. In principle, oxygen-anion diffusion can be enhanced in all oxides if the material can be doped with substitutional cations of lower formal charge relative to the cations in the parent compound.

High oxygen-anion mobility is desired in oxidation catalysts, supports for oxidation catalysts, oxygen transport membranes, solid-state electrolytes, oxygen sensors and other applications in which rapid transport of oxygen to or from a source is desired. Perovskites were investigated by Voorhoeve, Remeika and Trimble for reduction of oxides of nitrogen in automotive catalytic converters already in the early 1970s [21]. They had tested many perovskite materials including parent compounds $LaCoO_3$ and $LaMnO_3$ doped with Sr^{2+}, K^{1+}, Na^{1+} or Rb^{1+} for formation of oxygen-anion vacancies. They also investigated perovskites containing noble metals such as $La_{0.8}K_{0.2}Mn_{0.94}Ru_{0.06}O_{3-\delta}$ and $La_{0.8}K_{0.2}Mn_{0.9}Rh_{0.1}O_{3-\delta}$ [21]. With increased cost of noble metals dispersed on traditional supports, there has been renewed interest in perovskite catalysts for use in three-way automotive catalysts as a means to conserve noble metals [39–53]. Noble metals have long shown high activity for reduction of oxides of nitrogen [54]. Perovskites can be mixed and designed for complete oxidation of CO, hydrocarbons and soot as well as for decomposition and reduction of oxides of nitrogen [21,49].

Researchers have employed perovskite catalysts for both the complete or partial oxidation of hydrocarbons [55–58], including diesel fuel [55] and the military JP-8 fuel [57]. Liu and Krumpelt use Ru in some of their perovskite catalysts for partial oxidation of diesel fuel into synthesis gas for use in

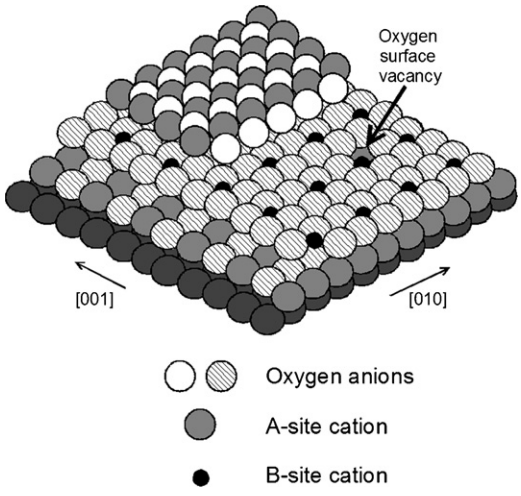

Fig. 18. An ideal perovskite (1 0 0) surface. Note oxygen surface vacancy.

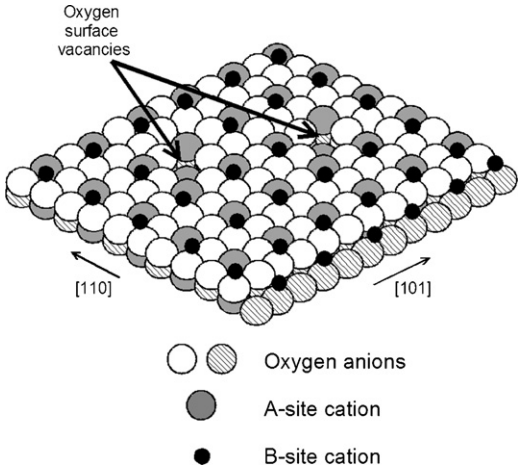

Fig. 19. An ideal perovskite (1 1 1) surface.

fuel cells [55]. Ruthenium is another catalyst long used in Fischer-Tropsch synthesis [11], and Ru is predicted to catalyze the reverse reactions converting hydrocarbons into synthesis gas. Shekhawat et al. have reviewed the field of catalysis for liquid fuel reforming for fuel cell use and discuss many types of catalysts for this application, such as hexaaluminates, in addition to perovskites [59].

Doping of perovskites to create oxygen-anion vacancies in the bulk of oxide materials will also create oxygen-anion vacancies on the surfaces of such materials. The ideal perovskite (1 0 0) and (1 1 1) surfaces [60] showing surface-anion vacancies are portrayed schematically in Figs. 18 and 19, respectively. The surface oxygen vacancies may act as active sites for the adsorption and dissociation of molecular oxygen. However, atomic steps [61], adatoms, edge sites and corner sites also likely form active sites for adsorption of molecular oxygen and hydrocarbons.

Desorption of molecular oxygen at elevated temperatures may create additional oxygen-anion vacancies in the perovskite lattice. In the case of perovskites incorporating cobalt or iron, some Co^{3+} and Fe^{3+} in the lattice may be reduced to Co^{2+} and Fe^{2+}, respectively, creating electron holes in the lattice, which allow high electron mobility in the perovskites [62,63]. Doping of materials such as $LaCoO_3$ with Sr^{2+} may create oxygen-anion vacancies but alternatively may lead to the oxidation of some Co^{3+} to Co^{4+} according to Voorhoeve et al. [21]. This also creates electron holes and additional pathways for conduction of electrons. Many perovskites can be designed to become mixed conductors, transporting electric charge by mobility of both electrons and oxygen anions, O^{2-} [62–64]. Perovskites can be insulators, semiconductors or true metallic conductors [6,21,62,63]. High electron mobility may be desired for some catalytic charge-transfer reactions [21], especially the difficult reduction step: $O_2 + 4e^- = 2O^{2-}$. High oxygen-anion mobility is desired for oxygen transfer.

4. Conclusions and future work

Thermodynamics implies that the formation of synthesis gas from the hydrocarbons in diesel fuel will be overwhelmingly favored if one atom of oxygen is added for each atom of carbon in the fuel and if the reaction mixture can be brought to equilibrium above about 950 °C. This temperature is higher relative to that required to reform methane and simple alkanes due to the lower H:C atomic ratio in diesel fuel. Thermodynamics also predicts that carbon will be favored at lower temperatures, and that the cracking of diesel fuel into carbon as fuel is heated will be a major issue in reforming. By enhancing the partial pressure of oxygen near inner reactor walls by effusing air into reactors through porous walls, membrane reactors show promise for suppressing deposition of carbon in the cool zones of reactors. Porous yttria-stabilized zirconia tubes were chosen to allow repeated thermal cycling, to minimize potential contamination of fuel cell catalysts by impurities originating from reactor walls and to provide adequate oxygen in a compact unit, which cannot be easily obtained using dense oxygen transport membranes.

In the search for low-cost diesel fuel reforming catalysts, which are stable to above 950 °C, which are tolerant to 15 ppm by mass sulfur in diesel fuel, and which can be cycled between reaction conditions and exposure to air, perovskites based upon iron and cobalt have been investigated. Both cobalt and iron show considerable catalytic activity for reverse Fischer-Tropsch reactions converting hydrocarbons into $H_2 + CO$ when operated above 950 °C. In preliminary studies, $La_{0.5}Sr_{0.5}CoO_{3-\delta}$ and $La_{0.5}Sr_{0.5}FeO_{3-\delta}$, were tested in the reactor hot zone to replace expensive Pd–Rh wire gauze. These perovskites were designed to contain oxygen anion vacancies to allow rapid diffusion of oxygen through the bulk materials and to attack adsorbed carbon from beneath. The materials are also mixed conductors, having high conductivity for electrons needed in electron transfer reactions. The perovskites are very stable in air at high temperatures (>1200 °C) and can catalyze complete oxidation of diesel fuel into CO_2 and water. However, perovskites can be reduced if the partial pressure of oxygen is too low. Literature studies imply that the walls of the membrane reactors must maintain partial pressure of oxygen near the perovskite catalysts of greater than 1×10^{-7} bar (1×10^{-2} Pa) for the parent cobalt compound, $LaCoO_3$, and above 1×10^{-17} bar (1×10^{-12} Pa) for the parent iron compound, $LaFeO_3$ [27]. The strontium-doped materials, because of higher mobility of oxygen, will require higher partial pressures of oxygen to remain stable. The iron-based perovskites are considerably more stable relative to the cobalt compounds [27]. The literature on cobalt and iron-based perovskites for the conversion of hydrocarbons into synthesis gas is extensive [65–72], as is the use of perovskites and other ceramics in catalytic membrane reactors [73–80]. Perovskites can be synthesized containing both Fe and Co in the same crystal lattice and containing additives such as Ce and Ru for enhancing oxidation of aromatic compounds. The many possibilities for designing perovskite catalysts by wide substitution of elements into both the A and B crystal lattice sites offer promise for their use in reforming diesel fuel.

Reaction of sulfur with lanthanum, strontium and calcium is a concern, and issues associated with other potential catalyst poisons such as phosphorous in diesel fuel require further

investigation. The strong affinity of La, Sr and Ca (and also Ce) for sulfur may temporarily protect Fe and Co from poisoning (until the system is saturated with sulfur). Because of the extreme stability of perovskites to oxidation, regeneration by oxidation may be a possibility, and sulfur may be removed as SO_2, for example. Assuming that perovskite catalysts can tolerate 15 ppm by mass sulfur in diesel fuel, issues remain concerning the poisoning of the nickel catalysts in SOFCs. Sulfur may need to be removed from the synthesis gas by methods such as warm-gas clean-up, likely using regenerable sorbents containing elements such as Ce, Ca, Mg, Mn, etc., which have the strongest affinity for sulfur (see Fig. 5). Alternatively, the fuel cell catalysts would need to return to use of noble metals such as Pt (see Fig. 5), a costly option, and the fuel cells operated above about 950 °C, which would also aid suppression of deposition of carbon (see Fig. 2).

Present results are preliminary, and considerable effort will be required to produce a commercially viable device for reforming diesel fuel into synthesis gas. External heat is now applied, and considerable parasitic power for fuel pumps and compressed air is consumed. Calculations imply that the heat released from partial oxidation of diesel fuel into $H_2 + CO$ will just barely be sufficient to heat fuel and air to desired reaction temperatures above 950 °C. Practical automotive diesel fuel reformers will need to be almost perfectly insulated or heat from other sources will need to be utilized to avoid consuming excess fuel to heat the reactants to the desired reforming temperatures. Alternatively, fuel cell exhaust may need to be recirculated into fuel reformers to utilize heat and to allow lower reformer temperatures by increasing the H:C and O:C atomic ratios in the reformer.

Acknowledgements

Authors thank the U.S. Department of Energy for funding (DE-FG02-05ER84394) and the Small Business Innovative Research Program for previous funding. Authors thank Vivian P. Knaus for preparation of figures and the manuscript.

References

[1] S.N. Paglieri, J.D. Way, Innovations in palladium membrane research, Sep. Purif. Methods 31 (1) (2002) 1–169.
[2] S.N. Paglieri, Palladium membranes, in: A.F. Sammells, M.V. Mundschau (Eds.), Nonporous Inorganic Membranes, Wiley-VCH, Weinheim, 2006, pp. 77–106.
[3] M.V. Mundschau, X. Xie, C.R. Evenson IV, Superpermeable hydrogen transport membranes, in: A.F. Sammells, M.V. Mundschau (Eds.), Nonporous Inorganic Membranes, Wiley-VCH, Weinheim, 2006, pp. 107–138.
[4] M.V. Mundschau, Hydrogen separation using dense composite membranes. Part 1. Fundamentals, in: A. Bose (Ed.), Inorganic Membranes for Energy and Fuel Applications, Springer, 2008 (Chapter 8).
[5] M.V. Mundschau, Catalytic Membrane Reactor and Method for Production of Synthesis Gas, U.S. Patent Application Filed, September 6, 2007.
[6] F.S. Galasso, Structure, Properties and Preparation of Perovskite-type Compounds, Pergamon Press, Oxford, 1969.
[7] C. Kittel, Introduction to Solid State Physics, 1st ed., John Wiley and Sons, New York, 1956, p. 78.
[8] H.W. Katz (Ed.), Solid State Magnetic and Dielectric Devices, John Wiley and Sons, New York, 1959, p. 77.
[9] Hans Jürgen Rösler, Lehrbuch der Minerologie, VEB Deutscher Verlag für Grundstoffindustrie, Leipzig, 1987, p. 391.
[10] R.B. Anderson, The Fischer-Tropsch Synthesis, Academic Press, Orlando, 1984.
[11] A. Steynberg, M. Dry (Eds.), Fischer-Tropsch Technology, Elsevier, Amsterdam, 2004.
[12] G.A. Olah, Á. Molnár, Hydrocarbon Chemistry, Wiley, New York, 1995.
[13] N.J. Bunce, Environmental Chemistry, Wuerz Publishing, Winnipeg, 1990 , p. 75.
[14] R. Diesel, Theorie und Konstruktion eines rationellen Wärmemotors, reprinted, in: R.H. Phelps, J.M. Stein (Eds.), The German Scientific Heritage, Holt, Rinehart and Winston, New York, 1962, pp. 131–146.
[15] J.G. Smith, Hydrocarbon Fuels, in: K.R. Williams (Ed.), An Introduction to Fuel Cells, Elsevier, Amsterdam, 1966, pp. 214–247.
[16] L.S. Darken, R.W. Gurry, Physical Chemistry of Metals, McGraw-Hill, New York, 1953, p. 361.
[17] D.W. Hopkins, Physical Chemistry and Metal Extraction, Macmillan, New York, 1954, p. 115.
[18] P. Davies, R.T. Donald, N.H. Harbord, in: M.V. Twigg (Ed.), Catalyst Handbook, 2nd ed., Manson Publishing, London, 1997 (Chapter 10).
[19] J.G. Smith, Solid Oxide Electrolytes, in: K.R. Williams (Ed.), An Introduction to Fuel Cells, Elsevier, Amsterdam, 1966, pp. 183–213.
[20] A.V. Kiselev, V.I. Lygin, Infrared Spectra of Surface Compounds, John Wiley and Sons, New York, 1975.
[21] R.J.H. Voorhoeve, J.P. Remeika, L.E. Trimble, Nitric oxide and perovskite-type catalysts: solid state and catalytic chemistry, in: R.L. Klimisch, J.G. Larson (Eds.), The Catalytic Chemistry of Nitrogen Oxides, Plenum, New York, 1975, pp. 215–233.
[22] L.V. Azároff, M.J. Buerger, The Powder Method in X-ray Crystallography, McGraw-Hill, New York, 1958 (Chapter 15).
[23] J.D.H. Donnay, G. Donnay, E.G. Cox, O. Kennard, M.V. King (Eds.), Crystal Data Determinative Tables, ACA Monograph Number 5, 2nd ed., American Crystallographic Association, Washington, DC, 1963.
[24] S. Lowell, J.E. Shields, Powder Surface Area and Porosity, Chapman and Hall, London, 1991.
[25] W.F. Libby, Promising catalyst for auto exhaust, Science 171 (1971) 499–500.
[26] L.A. Pederson, W.F. Libby, Unseparated rare earth cobalt oxides as auto exhaust catalysts, Science 176 (1972) 1355–1356.
[27] T. Nakamura, G. Petzow, L.J. Gauckler, Stability of the perovskite phase $LaBO_3$ (B = V, Cr, Mn, Fe, Co, Ni) in reducing atmosphere, Mater. Res. Bull. 14 (1979) 649–659.
[28] R.A. Outlaw, W.K. Peregoy, G.B. Hoflund, Permeation of Oxygen through High Purity, Large Grain Silver, NASA Technical Paper 2755, 1987.
[29] N.M.L.N.P Closset, R.H.E. van Doorn, H. Kruidhof, J. Boeijsma, About the Crystal Structure of $La_{1-x}Sr_xCoO_{3-\delta}$, as summarized JCPDS-International Centre for Diffraction Data, 48-0122 (1996).
[30] S.E. Dann, D.B. Currie, M.T. Weller, M.F. Thomas, A.D. Al-Rawwas, $La_{0.5}Sr_{0.5}FeO_3$, as summarized in: JCPDS-International Centre for Diffraction Data, 82-1962 (1997).
[31] S.E. Dann, D.B. Currie, M.T. Weller, M.F. Thomas, A.D. Al-Rawwas, The effect of oxygen stoichiometry on phase relations and structure in the system $La_{1-x}Sr_xFeO_{3-\delta}$ ($0 \leq x \leq 1$, $0 \leq \delta \leq 0.5$), J. Solid State Chem. 109 (1994) 134–144.
[32] I.S. Kotousova, S.M. Polyakov, Kristallografiya 17 (1972) 661 (as summarized in: JCPDS-International Centre for Diffraction Data, 71-0816).
[33] M. Mundschau, R. Vanselow, Phosphorus on platinum—field electron emission microscopy studies, Surf. Sci. 166 (1986) L131–L135.
[34] E. Savitsky, V. Polyakova, N. Gorina, N. Roshan, Physical Metallurgy of Platinum Metals, Mir Publishers, Moscow, 1978.
[35] L.G. Tejuca, J.L.G. Fierro, J.M.D. Tascón, Structure and reactivity of perovskite-type oxides, Adv. Catal. 36 (1989) 237–328.
[36] J. Sirman, The evolution of materials and architecture for oxygen transport membranes, in: A.F. Sammells, M.V. Mundschau (Eds.), Nonporous Inorganic Membranes, Wiley-VCH, Weinheim, 2006, pp. 165–184 (Chapter 6).

[37] A.F. Sammells, J.H. White, R. Mackay, Membranes for promoting partial oxidation chemistries, in: A.F. Sammells, M.V. Mundschau (Eds.), Nonporous Inorganic Membranes, Wiley-VCH, Weinheim, 2006, pp. 185–214 (Chapter 7).
[38] M. Carolan, Syngas membrane engineering design and scale-up issues. Application of ceramic oxygen conducting membranes, in: A.F. Sammells, M.V. Mundschau (Eds.), Nonporous Inorganic Membranes, Wiley-VCH, Weinheim, 2006, pp. 215–244 (Chapter 8).
[39] G. Saracco, V. Serra, V. Specchia, A. Delmastro, M. Vallino, F. Abbattista, Simultaneous abatement of diesel soot and NO_x by perovskite-type catalysts, in: K.S. Ramesh, M. Misono, P.L. Gai (Eds.), Catalyst Materials for High-Temperature Processes, American Ceramic Society, Westerville, Ohio, 1997, pp. 27–38.
[40] M. Misono, N. Mizuno, Design of catalysts based on perovskite-type mixed oxides, in: K.S. Ramesh, M. Misono, P.L. Gai (Eds.), Catalyst Materials for High-temperature Processes, American Ceramic Society, Westerville, Ohio, 1997, pp. 67–83.
[41] M. Misono, A view on the future of mixed oxide catalysts: the case of heteropolyacids (polyoxometalates) and perovskites, Catal. Today 100 (2005) 95–100.
[42] T. Screen, Platinum group metal perovskite catalysts, Platinum Met. Rev. 51 (2) (2007) 87–92.
[43] N.K. Labhsetwar, A. Watanabe, R.B. Biniwale, R. Kumar, T. Mitsuhashi, Alumina supported, perovskite oxide based catalytic materials and their auto-exhaust application, Appl. Catal. B: Environ. 33 (2001) 165–173.
[44] H. Tanaka, M. Uenishi, M. Taniguchi, I. Tan, K. Narita, M. Kimura, K. Kaneko, Y. Nishihata, J. Mizuki, The intelligent catalyst having the self-regenerative function of Pd, Rh and Pt for automotive emissions control, Catal. Today 117 (2006) 321–328.
[45] R. Bradow, D. Jovanović, S. Petrović, Ž. Jovanović, A. Terlecki-Baričević, Ruthenium perovskite catalysts for lean NO_x automotive emission control, Ind. Eng. Chem. Res. 34 (1995) 1929–1932.
[46] K. Zhou, H. Chen, Q. Tian, Z. Hao, D. Shen, X. Xu, Pd-containing perovskite-type oxides used for three-way catalysts, J. Mol. Catal. A: Chem. 189 (2002) 225–232.
[47] Y. Nishihata, J. Mizuki, T. Akao, H. Tanaka, M. Uenishi, M. Kimura, T. Okamoto, N. Hamada, Self-regeneration of a Pd-perovskite catalyst for automotive emissions control, Nature 418 (2002) 164–167.
[48] H. Tanaka, I. Tan, M. Uenishi, M. Kimura, K. Dohmac, Regeneration of palladium subsequent to solid solution and segregation in a perovskite catalyst: an intelligent catalyst, Top. Catal. 16/17 (2001) 63–70.
[49] H. Tanaka, M. Taniguchi, N. Kajita, M. Uenishi, I. Tan, N. Sato, K. Narita, M. Kimura, Design of the intelligent catalyst for Japan ULEV standard, Top. Catal. 30/31 (2004) 389–395.
[50] M.A. Ulla, R.A. Migone, J.O. Petunchi, E.A. Lombardo, Surface chemistry and catalytic activity of $La_{1-x}Sr_xCoO_3$ perovskite (M = Sr or Th), J. Catal. 105 (1987) 107–119.
[51] T. Nakamura, M. Misono, Y. Yoneda, Reduction–oxidation and catalytic properties of $La_{1-x}Sr_xCoO_3$, J. Catal. 83 (1983) 151–159.
[52] M. Crepsin, W. Keith Hall, The surface chemistry of some perovskite oxides, J. Catal. 69 (1981) 359–370.
[53] D.B. Meadowcroft, Low-cost oxygen electrode material, Nature 226 (1970) 847–848.
[54] B. Rausenberger, M. Mundschau, W. Święch, W. Engel, A.M. Bradshaw, Investigation of the $NO + H_2$ reaction on Pt {1 0 0} with low-energy emission and reflection microscopy: PEEM studies, J. Chem. Soc., Faraday Trans. 92 (1996) 4815–4821.
[55] D.-J. Liu, M. Krumpelt, Activity and structure of perovskites as diesel-reforming catalysts for solid oxide fuel cells, Int. J. Ceram. Technol. 2 (4) (2005) 301–307.
[56] M. Krumpelt, S. Ahmed, R. Kumar and R. Doshi, Partial Oxidation Catalysts, U.S. Patent 6,110,861, August 29, 2000.
[57] P. Erri, P. Dinka, A. Varma, Novel perovskite-based catalysts for auto-thermal JP-8 fuel reforming, Chem. Eng. Sci. 61 (2006) 5328–5333.
[58] F. Gaillard, X. Li, M. Uray, P. Vernoux, Electrochemical promotion of propene combustion in air excess on perovskite catalyst, Catal. Lett. 96 (2004) 177–183.
[59] D. Shekhawat, D.A. Berry, T.H. Gardner, J.J. Spivey, Catalytic reforming of liquid hydrocarbon fuels for fuel cell applications, Catalysis 19 (2006) 184–253.
[60] V.E. Henrich, P.A. Cox, The Surface Science of Metal Oxides, Cambridge University Press, Cambridge, 1996, pp. 36–42.
[61] M. Mundschau, E. Bauer, W. Święch, Modification of atomic steps by adsorbates observed by low energy electron microscopy and photoemission microscopy, Catal. Lett. 1 (1988) 405–412.
[62] J.B. Goodenough, Localized to Itinerant Electronic Transition in Perovskite Oxides, Springer, Berlin, 2001.
[63] N. Tsuda, K. Nasu, A. Fujimori, K. Siratori, Electronic Conduction in Oxides, Springer, Berlin, 2000.
[64] E. Dagotto, Nanoscale phase separation and colossal magnetoresistance. The physics of manganites and related compounds, Springer, Berlin, 2003.
[65] Y. Teraoka, H.-M. Zhang, S. Furukawa, N. Yamazoe, Oxygen permeation through perovskite-type oxides, Chem. Lett. Jpn. (1985) 1743–1746.
[66] Y. Teraoka, T. Nobunaga, N. Yamazoe, Effect of cation substitution on the oxygen semipermeability of perovskite-type oxides, Chem. Lett. Jpn. (1988) 503–506.
[67] Y. Teraoka, H.M. Zhang, K. Okamoto, N. Yamazoe, Mixed ionic–electronic conductivity of $La_{1-x}Sr_xCo_{1-y}Fe_yO_{3-\delta}$, Mater. Res. Bull. 23 (1988) 51–58.
[68] S. Cimino, S. Colonna, S. De Rossi, M. Faticanti, L. Lisi, I. Pettiti, P. Porta, Methane combustion and CO oxidation on zirconia-supported La, Mn oxides and $LaMnO_3$ perovskite, J. Catal. 205 (2002) 309–317.
[69] C. Oliva, L. Forni, A. D'Ambrosio, F. Navarrini, A.D. Stepanov, Z.D. Kagramanov, A.I. Mikhailichenko, Characterisation by EPR and other techniques of $La_{1-x}Ce_xCoO_{3+\delta}$, Appl. Catal. A: Gen. 205 (2001) 245–252.
[70] J. Kirchnerova, M. Alifanti, B. Delmon, Evidence of phase cooperation in the $LaCoO_3$–CeO_2–Co_3O_4 catalytic system in relation to activity in methane combustion, Appl. Catal. A: Gen. 231 (2002) 65–80.
[71] C. Oliva, L. Forni, A.V. Vishniakov, Spin glass formation in $La_{0.9}Sr_{0.1}CoO_3$ catalyst for flameless combustion of methane, Spectochim. Acta: Part A 56 (2000) 301–307.
[72] L.A. Isupova, G.M. Alikina, S.V. Tsybulya, A.N. Salanov, N.N. Boldyreva, E.S. Rusina, I.A. Ovsyannikova, V.A. Rogov, R.V. Bunina, V.A. Sadykov, Honeycomb-supported perovskite catalysts for high-temperature processes, Catal. Today 75 (2002) 305–315.
[73] U. Balachandran, J.T. Dusek, S.M. Sweeney, R.B. Poeppel, R.L. Mieville, P.S. Maiya, M.S. Kleefisch, S. Pei, T.P. Kobylinski, C.A. Udovich, A.C. Bose, Methane to syngas via ceramic membranes, Am. Ceram. Soc. Bull. 74 (1995) 71–75.
[74] W. Jin, S. Li, P. Huang, N. Xu, J. Shi, Y.S. Lin, Tubular lanthanum cobaltite perovskite-type membrane reactors for partial oxidation of methane to syngas, J. Membr. Sci. 166 (2000) 13–22.
[75] J.E. ten Elshof, H.J.M. Bouwmeester, H. Verweij, Oxygen transport through $La_{1-x}Sr_xFeO_{3-\delta}$ membranes. I. Permeation in Air/He gradients, Solid State Ionics 81 (1995) 97–109.
[76] C.-Y. Tsai, A.G. Dixon, Y.H. Ma, W.R. Moser, M.R. Pascucci, Dense perovskite, $La_{1-x}A'_xFe_{1-y}Co_yO_{3-\delta}$ (A′ = Ba, Sr, Ca), membrane synthesis, applications, and characterization, J. Am. Ceram. Soc. 81 (1998) 1437–1444.
[77] S. Li, W. Jin, N. Xu, J. Shi, Synthesis and oxygen permeation properties of $La_{0.2}Sr_{0.8}Co_{0.2}Fe_{0.8}O_{3-\delta}$ membranes, Solid State Ionics 124 (1999) 161–170.
[78] M.A. Hayward, M.J. Rosseinsky, Anion vacancy distribution and magnetism in the new reduced layered Co(II)/Co(I) phase $LaSrCoO_{3.5-x}$, Chem. Mater. 12 (2000) 2182–2195.
[79] L.M. van der Haar, H. Verweij, Homogeneous porous perovskite supports for thin dense oxygen separation membranes, J. Membr. Sci. 180 (2000) 147–155.
[80] W. Jin, S. Li, P. Huang, N. Xu, J. Shi, Fabrication of $La_{0.2}Sr_{0.8}Co_{0.2}Fe_{0.8}O_{3-\delta}$ mesoporous membranes on porous supports from polymeric precursors, J. Membr. Sci. 170 (2000) 9–17.